Xue, Y. et al. (2018) Arabidopsis blue light receptor phototropin 1 undergoes blue light-induced activation in membrane microdomains. Molecular Plant, 11(6), pp. 846-859.

There may be differences between this version and the published version. You are advised to consult the publisher's version if you wish to cite from it.

http://eprints.gla.ac.uk/161771/

Deposited on: 30 July 2018

Enlighten – Research publications by members of the University of Glasgow
http://eprints.gla.ac.uk

Arabidopsis Blue Light Receptor Phototropin 1 Undergoes Blue Light-Induced Activation in Membrane Microdomains

Yiqun Xue[1,2,8], Jingjing Xing[1,2,8], Yinglang Wan[1,8], Xueqin Lv[1], Lusheng Fan[3], Yongdeng Zhang[4], Kai Song[1,2], Li Wang[1], Xiaohua Wang[1], Xin Deng[1], Frantisek Baluska[5], John M. Christie[6], Jinxing Lin[1,7*]

[1]Institute of Botany, Chinese Academy of Sciences, Beijing 100093, China

[2]University of Chinese Academy of Sciences, Beijing 100049, China

[3]Department of Botany and Plant Sciences, University of California, Riverside, CA 92521, USA

[4]Department of Cell Biology, Yale University School of Medicine, New Haven, Connecticut 06520, USA

[5]Institute of Cellular and Molecular Botany, University of Bonn, Bonn, D-53115, Germany

[6]Institute of Molecular, Cell and Systems Biology, University of Glasgow, Bower Building, Glasgow, G12 8QQ, UK

[7]College of Biological Sciences and Biotechnology, Beijing Forestry University, Beijing 100083, China

[8]Y.X., J.X., and Y.W. contributed equally to this work.

[*]**Correspondence: Jinxing Lin (linjx@ibcas.ac.cn.)**

Running title: Activation of phototropin 1 in membrane microdomains

SUMMARY

Using single-molecule analysis techniques, we found that blue light can affect dynamic behavior of phototropin 1 (phot1) receptor kinase in a dose-dependent manner. Phosphorylation of functional phot1 in membrane microdomains, which is required for receptor signaling, occurred following light-driven receptor dimerization to promote faster rates of diffusion. All together, these findings support the hypothesis that phot1 recruitment to membrane microdomains serves as signaling platforms for this plant blue light receptor.

ABSTRACT

Phototropin (phot)-mediated signaling initiated by blue light (BL) plays a critical role in optimizing photosynthetic light capture at the plasma membrane (PM) in plants. However, the mechanisms underlying the regulation of phot activity at the PM in response to BL remain largely unclear. In this study, by single-particle tracking and step-wise photobleaching analysis we demonstrated that in the dark phot1-GFP proteins remain in an inactive state and mostly present as a monomer. The phot1-GFP diffusion rate and its dimerization increased in a dose-dependent manner in response to BL. In contrast, BL did not affect the lateral diffusion of kinase-inactive phot1^{D806N}-GFP, whereas it did enhance its dimerization, suggesting that phot1 dimerization is independent of its phosphorylation. Förster resonance energy transfer-fluorescence lifetime imaging microscopy (FRET-FLIM) analysis revealed that the interaction between phot1-GFP and AtRem1.3-mCherry was enhanced along with increased time of BL treatment. However, the BL-dependent interaction was not obvious in plants co-expressing phot1^{D806N}-GFP and AtRem1.3-mCherry, implicating that BL facilitated the translocation of functional phot1-GFP into AtRem1.3-labeled microdomains to activate phot-mediated signaling. Conversely, sterol depletion attenuated phot1-GFP dynamics, dimerization, and phosphorylation. Taken together, these results indicate that membrane microdomains act as an organizing platform essential for proper function of activated phot1 at the PM.

Key words: phot1, VA-TIRFM, spatiotemporal dynamics, blue light signaling, membrane microdomains

INTRODUCTION

Phototropins (phots) play key roles in phototropism, chloroplast movement, stomatal opening, leaf expansion, and solar tracking in response to blue light (Christie, 2007). *Arabidopsis thaliana* has two phots, phot1 and phot2, with overlapping but not completely redundant physiological functions (Liscum and Briggs, 1995; Sakai et al., 2001; Christie, 2007; Mo et al., 2015). Physiological processes mediated by phot1 and phot2 are therefore complex.

Studies on understanding phot functions have so far focused on their individual signaling mechanisms, as well as their biophysical and structural properties. These studies have shown that phots are plasma membrane (PM)-associated receptor kinases with two photosensory input regions, known as LOV1 (Light, Oxygen, Voltage sensing 1) and LOV2, located at the N-terminus coupled to a serine/threonine (Ser/Thr) kinase domain at the C-terminus (Christie, 2007; Matsuoka et al., 2007). In dark-grown (DG) *Arabidopsis* seedlings, phot1 is expressed broadly throughout the seedling, with strong expression in the hypocotyl hook and elongation zone (Sakamoto and Briggs, 2002; Wan et al., 2008). Phot1 is associated with the inner surface of the PM by an attachment mechanism that is still not fully understood. BL excitation induces intermolecular interactions between phot1 molecules and a rapid, but partial, internalization of the photoreceptor into the cytoplasm in response to autophosphorylation (Sakamoto and Briggs, 2002; Wan et al., 2008; Kaiserli et al., 2009; Hohm et al., 2013). BL-induced autophosphorylation is considered the primary step for phototropin-mediated signaling, since the kinase-inactive mutant phot1^{D806N} abolishes phot1 signaling and function (Inoue et al., 2008; Kaiserli et al., 2009). Both myristoylation and farnesylation modifications, which effectively prevent phot1 internalization, do not appear to impair phototropism and phot1 function in *Arabidopsis*, indicating that phot1 signaling initiates at the PM (Preuten et al., 2015). Yet, how phot1 activation and signaling are spatially coordinated at the PM, and the relationships between these processes, remain poorly resolved.

Owing to the heterogeneous and highly dynamic nature of the PM, it is important to analyze the behaviors of individual membrane molecules and their interactions over time. Recently, single-particle techniques have been developed to analyze the spatiotemporal dynamics of specific molecules and their interactions in intact plant cells (Li et al., 2013; Wang et al., 2015). We previously reported that phot1 fused to green fluorescent protein (GFP) can be easily observed by variable-angle total internal reflection fluorescence microscopy (VA-TIRFM) in intact *Arabidopsis* seedlings (Wan et al., 2011). In the present study, we applied single-particle imaging and tracking methods, step-wise photobleaching analysis, as well as biochemical assays to determine the dynamic behavior, molecular interactions, and protein phosphorylation of phot1-GFP under different BL conditions. As phot1 was detected in the detergent-resistant membrane (DRM) fraction from plants (Demir et al., 2013), we also explored whether phot1-mediated signaling in response to BL involves membrane microdomains. Our comprehensive analyses provide new insights into the regulatory mechanism of phot-mediated signaling at the PM and support the hypothesis that phot1 recruitment to membrane microdomains serves as a signaling platform for this plant blue light receptor.

RESULTS

Spatiotemporal Dynamics and Oligomeric States of Phot1-GFP at the PM in Darkness

To examine the spatiotemporal dynamics of phot1 at the PM in response to BL, we used transgenic *Arabidopsis* expressing a PHOT1-GFP fusion protein driven by the native *PHOT1* promoter in the *phot1-5* mutant background. When examining the distribution of phot1-GFP in 4-day old DG seedlings, we found that phot1-GFP mostly localizes at the PM in hypocotyl epidermal cells. After BL irradiation, a fraction of phot1-GFP is released from the PM and rapidly internalized, confirming that it responds to BL (Supplemental Figure 1).

Single-particle analysis provides higher spatial resolution and signal/noise ratio than laser scanning confocal microscopy; thus, individual fluorescent particles of phot1-GFP can be clearly visualized at the PM of hypocotyl epidermal cells in the dark-grown (DG) seedlings (Figure 1A and Supplemental Movie 1). Using a single-particle tracking (SPT) algorithm, we found some spots showed highly dynamic behaviors with short membrane dwell times (< 2 s, spots highlighted by magenta and green circles), whereas other spots existed in the visual field for longer periods (> 10 s, spots highlighted by orange and blue circles) (Figure 1B and 1C). The frequency distribution of surface dwell time values showed that the curves could be fitted to an exponential function and the τ value was 5.48 s in DG seedlings (Figure 1D). The distribution of diffusion coefficients or motion ranges measured based on the trajectories of phot1-GFP spots was plotted on histograms and fitted to a Gaussian function to characterize the global mobility; the Gaussian peaks (noted as $\hat{G}$) were defined as the characteristic values. Under DG conditions, the diffusion coefficients of phot1-GFP were distributed in two populations with $\hat{G}_D$ values of $1.05 \pm 0.14 \times 10^{-4}$ $\mu m^2/s$ (32.2%) and $3.16 \pm 0.46 \times 10^{-3}$ $\mu m^2/s$ (67.8%) (Figure 1E). The motion ranges of phot1-GFP distributed in a single population with a $\hat{G}_M$ value of 0.398 ± 0.008 μm (indicating short-distance motion) (Figure 1F). These results indicate that the dynamics of phot1 movement are heterogeneous at the PM.

Since GFP-labeled phot1 was excited with 473 nm light, which can activate the photoreceptor, this blue light exposure may affect the measurements of phot1 dynamics. To address this concern, we generated transgenic lines expressing a phot1-mCherry fusion driven by the 35S promoter in the *phot1-5* background. The transgene restored normal phototropic bending, indicating that it retains phot1 function (Supplemental Figure 2A). As a control, we determined the dynamic parameters of phot1-mCherry in hypocotyl cells under DG conditions and found that the τ value of surface dwell time curve was 5.56 s when excited with 561 nm light, a wavelength that is not absorbed by phot1. We found that the diffusion coefficients of

phot1-mCherry were distributed into two populations and the motion ranges were distributed in a single population showing short-distance motion (Supplemental Figure 2B–2D), in agreement with the data obtained for phot1-GFP. These results demonstrated that excitation with 473 nm light did not affect the dynamics of GFP-labeled phot1 in DG conditions.

In sequential images, we observed two phot1-GFP particles diffusing laterally along the membrane, colliding, and then fusing together (Supplemental Figure 3A–3D and Supplemental Movies 2 and 3). To distinguish the number of phot1-GFP molecules contained in these diffraction-limited fluorescent spots, we performed calibration experiments using monomeric GFP (mGFP) obtained from a previous study (Song et al., 2017). Based on the fluorescence intensity of individual mGFP spots (Song et al., 2017), we used mGFP as a standard to analyze the fluorescence intensity for those particles before and after fusions. We found the intensity of phot1 increased to approximately two times of original spots after fusion (Supplemental Figure 3E and 3F), indicating the occurrence of phot1 dimerization.

As the photobleaching steps and fluorescence intensities of fluorescent proteins reflect the oligomeric states of the target proteins (Das et al., 2007; Ulbrich and Isacoff, 2007), we further quantified the dimerization rates of phot1-GFP molecules using two algorithms. By applying the “Progressive Idealization and Filtering” (PIF) program (McGuire et al., 2012), we found that most of the spots underwent one-step and two-step bleaching, reflecting the monomeric and dimeric states of phot1-GFP molecules, respectively (Supplemental Figure 3G). Under DG conditions, phot1-GFP monomers and dimers accounted for 92.8% and 7.2% of fluorescent spots (Figure 1G). By applying a spatial intensity distribution analysis (SpIDA) algorithm to examine the distribution of oligomers in a single image (Godin et al., 2011), we found that the monomer density was 3.01 ± 0.47 μm^{-2} and the dimer density was 0.23 ± 0.1 μm^{-2} under DG conditions (Figure 1G). These results suggested that phot1 exists mainly as a monomer under DG conditions.

Light-induced Changes in Phot1-GFP Dynamics and Oligomerization Status at the PM

Ligand binding often causes a change in the receptor environment and induces a change in receptor mobility (Li et al., 2013; Sun et al., 2015). The dynamics of molecules binding to the PM can be assessed by measuring the time between the appearance and the disappearance of individual particles (Ueda et al., 2001; Wang et al., 2015). To investigate whether photostimulation affects phot1 dynamics, we examined phot1-GFP dwell times under different BL conditions. DG seedlings were first exposed to three different intensities of BL and then immediately observed by VA-TIRFM. When the curves for phot1-GFP dwell times under these regimes were fitted to exponential functions, the τ value was 4.83 s following 10 min of treatment with 0.1 μmol m^{-2} s^{-1} BL (BL-60 treatment, total fluence 60 μmol m^{-2}) and τ was 4.45 s after 10 min of treatment with 1.0 μmol m^{-2} s^{-1} BL (BL-600, total fluence 600 μmol m^{-2}) (Figure 2A). Treatment for 10 min with 10 μmol m^{-2} s^{-1} BL (BL-6000, total fluence 6000 μmol m^{-2}) resulted in a further decrease in the τ value to 3.95 s (Figure 2A). These data demonstrated that dwell times of phot1 at the PM decreased progressively as the BL intensity increased.

We also determined the diffusion coefficients and motion ranges of phot1-GFP spots at the different BL levels. In the BL-60 treatment, the distribution of diffusion coefficients yielded a single population and $\hat{G}_D$ was 1.98 ± 0.09 × 10^{-3} $\mu m^2/s$. In the BL-600 treatment, $\hat{G}_D$ increased to 3.02 ± 0.27 × 10^{-3} $\mu m^2/s$, and in the BL-6000 treatment, $\hat{G}_D$ further increased to 5.01 ± 0.33 × 10^{-3} $\mu m^2/s$ (Figure 2B). For the motion ranges of phot1-GFP, under the BL-60 treatment, there was one population in the distribution with $\hat{G}_M$ value 0.452 ± 0.004 μm, whereas in the BL-600 treatment, the histogram of motion ranges showed a bimodal distribution, in which 64.6% of the spots showed short-distance motion ($\hat{G}_M$ = 0.354 ± 0.009 μm) and 35.4% of the spots

showed relatively long-distance motion with a $\hat{G}_M$ of 0.627 ± 0.003 μm (Figure 2C). In the BL-6000 treatment, the percentage of long-distance motion increased to 60%. Since motion range was calculated as the longest distance a particle travelled within its lifetime or during the recording time, the bimodal distribution implied that some phot1 particles may be constrained in a small “yard”, while others are free to roam in a large “field”. These results demonstrated that BL induces phot1-GFP proteins to move faster and diffuse into wider regions.

To investigate the oligomerization state of phot1 at the PM upon irradiation with BL, we further calculated the dimerization rates of phot1 following BL treatment. Photobleaching step analysis showed that the dimerization rate of phot1-GFP increased to 15.2% following the BL-60 treatment, to 23.5% with BL-600 treatment, and to 35.5% with the BL-6000 treatment (Figure 2D). Three-step photobleaching was only observed in very rare cases (1 of 500 spots), and no instances of four or more bleaching steps were detected in any treatment. Therefore, phot1-GFP likely exists mainly as monomers and dimers at the PM and the dimerization rate increases upon blue light irradiation. Parallel studies using SpIDA showed that monomer density decreased significantly to 2.27 ± 0.18 μm^{-2} in the BL-60 treatment ($P < 0.001$), then to 1.94 ± 0.08 μm^{-2} in BL-600 ($P < 0.05$) and to 1.13 ± 0.10 μm^{-2} ($P < 0.001$) in BL-6000. The dimer density increased significantly to 0.44 ± 0.08 μm^{-2} following BL-60 treatment ($P < 0.01$), then to 0.56 ± 0.07 μm^{-2} with BL-600 ($P < 0.05$) and to 0.77 ± 0.08 μm^{-2} with BL-6000 ($P < 0.01$) (Figure 2E). These results showed that BL promotes phot1 dimerization in a dose-dependent manner.

Partitioning of Phot1-GFP is Associated with Membrane Microdomains

It has been suggested that the sterol-rich membrane microdomains are involved in cell and tissue polarity in plants, and these domains may modulate the partitioning and activity of some membrane proteins (Titapiwatanakun et al., 2009). We therefore used

AtRem1.3 as a marker of sterol-rich lipid environments at the *Arabidopsis* PM (Demir et al., 2013), and generated transgenic plants co-expressing phot1-GFP and AtRem1.3-mCherry. By analyzing the membrane distribution of phot1-GFP and AtRem1.3-mCherry with dual-color VA-TIRFM, we found some regions with clear fluorescence signals in both GFP and mCherry channels, indicating spatial overlap between phot1-GFP and AtRem1.3-mCherry foci (Figure 3A–3C and Supplemental Movies 6). The kymograph assembled from serial time-lapse images showed the localization of spots in both channels over time (Figure 3D and 3E). The intensity traces with different frame lengths further verify that co-diffusion of phot1-GFP and AtRem1.3-mCherry indeed occurred in living cells, indicating that phot1 is associated with AtRem1.3-labeled microdomains.

Equivalent experiments were performed on plants treated with methyl-β-cyclodextrin (MβCD) (Zidovetzki and Levitan, 2007), a sterol-disrupting reagent. Treatment with MβCD did not alter the PM distriubution of phot1-GFP (Supplemental Figure 4A and 4B; Supplemental Movies 5 and 6). However, MβCD induced quantiatively different changes in the confinement area and diffusion rate of phot1-GFP in contrast with untreated seedlings (Supplemental Figure 4C and 4D), even under DG conditions, when phot1 is still in the inactive state. In addition, we tested the phototropic response of DG wild-type seedlings treated with MβCD and found that seedlings did not reach a similar bending angle to those in the mock control during the directional BL irradiation period (Supplemental Figure 4F), indicating that MβCD treatment attenuates phototropism to BL. Because MβCD treatment efficiently depletes campesterol and β-sitosterol from membranes (Roche et al., 2008), and β-sitosterol probably plays a similar role to that of cholesterol in mammalian cells (Hartmann, 1998), we compensated for the loss of plasma membrane sterols by adding campesterol or β-sitosterol (100 μg/mL) to the cells following MβCD treatment and found a recovery of phot1 dynamics after sterol supplementation, indicating the specificity of MβCD in sterol depletion (Supplemental Figure 4E). Combined, our

sterol depletion and sterol supplementation experiments provide further support for the hypothesis that membrane microdomains are involved in partitioning phot1 at the PM.

Assembly of Phot1-GFP in Membrane Microdomains

Receptors can dimerize in membrane microdomains, inducing signal transduction (Corriden et al., 2014). Although we demonstrated that BL can induce phot1 dimerization, whether the activation occurred inside or outside membrane microdomains remained to be tested. During BL exposure, we observed two phot1-GFP spots that collided and became a single spot that co-localized with an AtRem1.3-mCherry spot (Figure 4A and 4B; Supplemental Movies 7). By counting 42 dimerization events of phot1-GFP, we found that 26 of the dimers co-localized with AtRem1.3-mCherry (60.5%). A parallel experiment using MβCD revealed that the percentage of phot1-GFP dimers was 21.1% after treatment (Figure 4C), which was significantly lower than that without MβCD treatment (35.51%, $P < 0.01$). Since the majority of phot1 dimers co-localized with AtRem1.3, and depleting membrane sterols by MβCD treatment attenuated BL-induced phot1 dimerization, we inferred that phot1 dimerization occurs within membrane microdomains.

We also quantified the levels of co-localization of phot1-GFP and AtRem1.3-mCherry by calculating the protein proximity index (PPI), which has been shown to yield good estimates of the fraction of co-localized molecules (Wu et al., 2010; Zinchuk et al., 2011). Seedlings were fixed before imaging to overcome the influence of the BL laser on phot1 activity during observation. PPI analysis can generate a 3D plot of phot1-GFP and AtRem1.3-mCherry cross-correlation versus pixel shift (Supplemental Figure 5A). The sharp peak at the center accounted for the specific colocalization. Under DG conditions, mean PPI values were 0.21 ± 0.03 for phot1-GFP to AtRem1.3-mCherry. After 10 μmol m^{-2} s^{-1} BL treatment for 1 min, the PPI values

increased to 0.29 ± 0.03 (P < 0.01) (Supplemental Figure 5B). These PPI values further increased when the BL treatment was extended to 5, 10, and 60 min, which gave PPI values of 0.31 ± 0.03, 0.39 ± 0.03, and 0.52 ± 0.06, respectively (Supplemental Figure 5B). These results showed an increasing level of co-localization between phot1-GFP and AtRem1.3-mCherry in response to BL irradiation, suggesting that phot1 is recruited to membrane microdomains in a BL dose-dependent manner.

Since co-localization is not a direct measure of interaction, we performed a FRET-FLIM assay, as previously described (Bucherl et al., 2014), to further verify the molecular interactions between phot1 and AtRem1.3. *In vivo* FRET-FLIM with potential enhanced nanometer-scale displacement detection facilitated our analysis of protein–protein interactions and provided high-accuracy quantitative analysis of spatial protein–protein correlations at the single-molecule level (Long et al., 2017). Under DG conditions, energy transfer from GFP (donor) to mCherry (acceptor) resulted in a decrease in the GFP lifetime from 2.508 ± 0.011 ns in phot1-GFP lines to 2.368 ± 0.011 ns in phot1-GFP AtRem1.3-mCherry lines (Figure 4D and 4E). By contrast, the GFP fluorescence lifetime did not decrease in the free-GFP AtRem1.3-mCherry lines (2.479 ± 0.018 ns), suggesting that phot1 interacts with AtRem1.3. The fluorescence lifetime of GFP decreased when seedlings were treated with 10 μmol m^{-2} s^{-1} BL for 1 min (2.323 ± 0.021 ns). Increasing the BL treatment time to 5, 10, and 30 min resulted in a further reduction in lifetime values to 2.308 ± 0.024 ns, 2.265 ± 0.018 ns, and 2.077± 0.020 ns, respectively (Figure 4F–4H). With BL treatment for 30 min, the mean fluorescence lifetime of free-GFP (2.487 ± 0.017 ns) showed no obvious difference from that of phot1-GFP alone, supporting the specific interaction between phot1 and AtRem1.3. These results demonstrated that BL can enhance the phot1–AtRem1.3 interaction in a time-dependent manner.

Phot1 Phosphorylation Following Its Dimerization is Connected with Membrane Microdomains

Previous studies showed that autophosphorylation is necessary for phot1 signal transduction (Inoue et al., 2008). In the present study, we established transgenic *Arabidopsis* lines carrying the *PHOT1*$_{PRO}$*::PHOT1*^{D806N}*-GFP* transgene, expressing kinase-inactive phot1, in the *phot1-5* mutant background (Supplemental Figure 6A). Although quantitative real-time PCR (qPCR) experiments showed that *PHOT1* expression in the phot1^{D806N}-GFP line was similar to that found in the phot1-GFP line (Supplemental Figure 6B), as reported previously (Inoue et al., 2008), the phot1^{D806N}-GFP fusion protein did not restore normal phototropic bending (Supplemental Figure 6C). Moreover, we found that the membrane distribution of phot1^{D806N}-GFP was similar to that of wild-type phot1-GFP in the root and hypocotyl cells of DG seedlings. In contrast to phot1-GFP, phot1^{D806N}-GFP was not internalized to the cytoplasm after illumination with BL (Supplemental Figure 6D), confirming that the D806N mutation of phot1-GFP abolished BL-induced relocalization of phot1.

As both the diffusion coefficients and motion ranges of phot1-GFP at the PM increased after BL exposure, we then examined these parameters in phot1^{D806N}-GFP expressing lines under DG or BL-6000 conditions by VA-TIRFM (Supplemental Movies 8 and 9). The diffusion coefficients of phot1^{D806N}-GFP in hypocotyl cells under BL-6000 conditions showed two populations with $\hat{G}_D$ values of 1.66 ± 0.31 × 10^{-4} $\mu m^2/s$ (40.7%) and 3.89 ± 0.51 × 10^{-3} $\mu m^2/s$ (59.3%), similar to those observed in DG seedlings with $\hat{G}_D$ values of 2.51 ± 0.42 × 10^{-4} $\mu m^2/s$ (38.5%) and 4.07 ± 0.52 × 10^{-3} $\mu m^2/s$ (61.5%) (Figure 5A) or as in DG phot1-GFP expressing seedlings (Figure 1E). Under BL-6000 conditions, the motion ranges of phot1^{D806N}-GFP spots were characterized by a single population with a $\hat{G}_M$ of 0.373 ± 0.008 μm (Figure 5B), similar to DG conditions with a $\hat{G}_M$ of 0.386 ± 0.006 μm, and to phot1-GFP spots under DG conditions (Figure 1F). These data showed that the distributions of lateral diffusion rates of kinase-inactive phot1 were similar under dark and light conditions,

suggesting that BL-induced dynamic changes were abolished in the kinase-inactive mutant.

Parallel experiments were also performed with fluorescence recovery after photobleaching (FRAP) assays to further verify the effects on lateral diffusion of the phot1^{D806N} kinase-inactive mutant in the DG hypocotyls. When regions of the PM were photobleached and the fluorescence intensity of recovery was measured over time (Figure 5C), FRAP signals at the center of the bleached areas were compared with those in the whole region or at the periphery of the bleached areas (Figure 5D). For phot1-GFP, recovery of fluorescence in the center of the bleached area was slower than that in the periphery or in the whole bleached area (Figure 5D). By contrast, in the phot1^{D806N}-GFP lines, these regions had similar kinetic profiles (Figure 5E), indicating that the lateral diffusion of phot1 was also abolished in the kinase-inactive mutant.

To detect intramolecular phot1 interactions in the presence or absence of BL irradiation, bimolecular fluorescence complementation (BiFC) was performed in tobacco epidermal cells. Phot1 or phot1^{D806N} was fused to either the N-terminus of yellow fluorescent protein (YFP) (phot1-nY or D806N-nY) or the C-terminus of YFP (phot1-cY or D806N-cY), and these constructs were divided into four combinations for analysis as shown in Figure 6A. In each case, fluorescence complementation of the fusion products was clearly detectable at the PM following BL irradiation, whereas the signal was not observed under dark conditions (Figure 6A) or in controls with phot1-nYFP or phot1^{D806N}-cYFP combined with cYFP (Supplemental Figure 7A). However, the mCherry fluorescence was always visible in both conditions (Supplemental Figure 7B). Quantification of YFP fluorescence intensity indicated that there were no significant differences in relative fluorescence intensity among the four groups after BL irradiation (Figure 6B), demonstrating that inactivation of phot1 kinase activity does not alter its light-driven molecular interaction. In an equivalent

experiment, the photobleaching step distribution of phot1^{D806N}-GFP spots in DG *Arabidopsis* hypocotyls showed that 91.1% were monomers and 8.9% were dimers. Dimer levels increased to 39.2% under BL-6000 conditions (Figure 6C), further demonstrating that the inhibition of phosphorylation has no effect on phot1 dimerization.

Since our sterol extraction experiments suggested that phot1 recruitment to membrane microdomains is involved in phototropism (Supplemental Figure 4F), we examined whether microdomains are related to phot1 phosphorylation. Using FRET-FLIM, we found a decrease in GFP lifetime in the transgenic plants coexpressing phot1^{D806N}-GFP and AtRem1.3-mCherry, as compared with phot1^{D806N}-GFP lines. The FRET efficiency (6.81 ± 0.95%) was similar to that between phot1-GFP and AtRem1.3-mCherry under dark conditions (5.57 ± 0.42%). In contrast to the enhanced interaction between phot1 and AtRem1.3, we found that the FRET efficiency between phot1^{D806N} and AtRem1.3 did not significantly change with increasing BL treatment time (Supplemental Figure 7C).

We used immunoblotting to detect the level of phosphorylation of phot1, as phosphorylated phot1 shifts to a lower electrophoretic mobility in SDS-PAGE than non-phosphorylated phot1 (Knieb et al., 2005). BL irradiation of DG seedlings resulted in phot1 phosphorylation, as evident by its reduced electrophoretic mobility (Figure 6D). In contrast, treatment of seedlings with MβCD prior to BL irradiation reduced the amount of phot1 that was phosphorylated (Figure 6D), indicating partial inhibition of phot1 phosphorylation following the disruption of membrane microdomains. This result was confirmed by a sterol complement experiment, showing that the magnitude of shifted phot1 recovered after addition of campesterol or β-sitosterol following MβCD treatment (Supplemental Figure 8). These results suggest that membrane microdomains serve as an integral determinant of phot1 functionality.

DISCUSSION

Signal perception through ligand-induced activation of membrane-localized receptors is a common feature among living organisms (Li et al., 2013). BL-induced phot1-mediated signaling at the PM initiates multiple signaling cascades, regulating processes that collectively optimize photosynthetic efficiency (Christie, 2007). However, the highly dynamic nature of PM proteins means that analyzing the dynamics and activation of phot1 molecules within living cells during BL treatment poses a challenge. Single-particle analysis can follow the trajectories of molecules and identify single events, transient interactions, or intermediates along these reaction pathways (Li et al., 2013; Tinoco and Gonzalez, 2011). Therefore, we applied these precise analyses with high spatial and temporal accuracy to characterize the dynamics of phot1 in *Arabidopsis* hypocotyl cells by VA-TIRFM. In this study, we found the individual phot1-GFP particles appear at the PM as isolated fluorescent spots and demonstrated dramatically different dynamics. Furthermore, we evaluated the spatial distribution and complex dynamics of phot1 in response to different BL fluence rates. Thus, our findings provide new insights into the regulation of photoreceptor dynamics at the PM and clarify the complex relationships between dynamic behavior and signal sensing.

Previously, it was reported that phot1 functions over a wide range of fluence rates of BL, mediating phototropism from 0.01 to 100 μmol m^{-2} s^{-1} (Sakai et al., 2001). In our study, we tested three fluence rates of BL (BL-60, BL-600, and BL-6000) to analyze the dynamic characteristics of phot1-GFP upon activation. By fitting the distribution of surface dwell time to an exponential function, we found that τ decreased gradually with the increasing fluence rates of BL, suggesting that BL induced dissociation of phot1-GFP from the PM. We further revealed that the diffusion coefficients and motion ranges of phot1-GFP spots increased progressively with increasing fluence rates of BL, leading to faster lateral diffusion. We found that phot1-GFP was distributed in the mature zone cells (non-growing regions where the hypocotyl does

not develop phototropic curvature) and its dynamics can change in response to blue light. However, no significant differences were found in the dynamics of phot1-GFP compared with those in elongation zone cells (the rapidly growing region of the hypocotyl where we detected movement of phot1) (Supplemental Figure 9). We suspected that BL signal transduction not only relies on phot1 status or dynamic changes, but also depends on the interaction between phot1 and other downstream proteins, which changes auxin transport and controls phototropism, as reported previously (Wan et al., 2012).

Proteins rarely act alone, and they generally undergo self-association to form homo-/heterodimers or homo-/heterooligomers following ligand stimulation (Schlessinger, 2002). Dimerization and oligomerization can produce structural and functional changes in proteins to potentiate downstream signaling (Marianayagam et al., 2004), and these changes may also influence receptor desensitization (George et al., 2000). In the present study, PIF analysis indicated that under dark conditions, 92.8 % of phot1-GFP spots exhibited one-step photobleaching, and the ratio of dimers increased significantly upon BL irradiation. In addition, SpIDA showed that monomer density decreased and dimer density increased upon BL irradiation. These results showed that inactive phot1 mostly exists as monomers, and the dimerization rates significantly increased with increasing BL exposure, providing strong evidence that BL can act as a physical ligand-like factor that induces phot1 dimerization at the PM in a dose-dependent manner.

PMs are partitioned into different types of membrane microdomains with various sizes and degrees of mobility (Jarsch et al., 2014). In plants, membrane microdomains enriched in sterols and sphingolipids have been implicated in many cellular processes (Malinsky et al., 2013; Yadeta et al., 2013). Demir et al. (2013) classified 120 proteins as putative membrane microdomain residents in plant DRMs, including phot1. Here, we found the co-diffusion of phot1-GFP and AtRem1.3-mCherry in living cells, and a 60.5% colocalization rate between dimerized phot1-GFP and AtRem1.3-mCherry in

the recorded dimerization events in the BL-6000 condition, suggesting that dimerization of phot1-GFP may occur in the membrane microdomains. Also, sterol extraction by MβCD altered the confinement area and diffusion rate of phot1-GFP and resulted in decreased rates of phot1 dimerization in response to BL. Moreover, we found that phot1 dynamics recovered after sterol supplementation, confirming the specificity of MβCD in sterol depletion. Importantly, we found via PPI analysis that there was an increased level of co-localization between phot1-GFP and AtRem1.3-mCherry in response to BL irradiation. FRET-FLIM analysis of phot1-GFP/AtRem1.3-mCherry dual-labeled lines further showed that there was energy transfer from phot1-GFP to AtRem1.3-mCherry under dark conditions, suggesting that phot1 interacts with AtRem1.3. Increasing the time of the blue light treatment resulted in a further reduction in GFP lifetime values, confirming that blue light led to a time-dependent increase of the phot1–AtRem1.3 interaction. Based on these results, we can conclude that photoactivation triggers the nanoscale aggregation of phot1 within preexisting microdomains.

Protein phosphorylation plays a role in a wide range of cellular processes, with many receptors switched on or off by phosphorylation and dephosphorylation (Ciesla et al., 2011). Previous studies showed that phosphorylation is necessary for phot1 signal transduction. Mutations in the phosphorylation sites, such as Ser-849 and Ser-851, resulted in defective phototropism, stomatal opening, leaf flattening, and chloroplast accumulation responses (Inoue et al., 2008). In tobacco leaves transiently expressing phot1^{D806N}-GFP, which lacks kinase activity, no internalization was observed in response to BL (Kaiserli et al., 2009). Our observations indicated that the D806N mutation of phot1-GFP abolished BL-induced phot1 relocalization and hypocotyl bending. By SPT analysis, we found no significant changes in the diffusion coefficient or motion range of phot1^{D806N}-GFP spots after BL pretreatment in comparison with phot1-GFP lines under DG conditions. FRAP analysis further indicated that the lateral diffusion in phot1^{D806N}-GFP lines was significantly slower than those in normal lines, implying that the BL-induced dynamic behaviors of phot1 were abolished in the

kinase-inactive mutant. These results demonstrating that phot1 phosphorylation appears to be essential for rapid phot1 diffusion.

Isolated LOV1 domains of phot1 form homodimers (Nakasako et al., 2004; Katsura et al., 2009), whereas the intermolecular phosphorylation of phot1 can occur in the absence of LOV1 (Kaiserli et al., 2009). LOV2 domains can dimerize in solution, depending on their concentration (Nakasako et al., 2004; Katsura et al., 2009). Our BiFC analysis showed the direct interaction between phot1^{D806N} molecules, demonstrating that inactivation of phot1 kinase activity does not alter its light-driven molecular interaction. In addition, examination of the photobleaching step distribution in phot1^{D806N}-GFP expressing transgenic lines also revealed an increase in the dimer rate after BL treatment, indicating that BL-induced phot1 dimerization does not require kinase activity. Based on these results, we concluded that phot1 dimerization is independent of phosphorylation and that these two events occur sequentially. In addition, we found that there was an energy transfer from phot1^{D806N}-GFP to AtRem1.3-mCherry under dark conditions, but increasing the time of blue light treatment did not significantly affect FRET efficiency between phot1^{D806N}-GFP and AtRem1.3-mCherry, indicating that inactivated phot1^{D806N}-GFP can interact with AtRem1.3, which is similar to inactivated phot1-GFP, whereas blue light does not cause the time-dependent increase in the phot1^{D806N}–AtRem1.3 interaction, confirming that the phot1–AtRem1.3 interaction depends on phot1 function. Given our findings that phot1 may dimerize within membrane microdomains before receptor phosphorylation, together with the partial inhibition of phot1 phosphorylation following the disruption of membrane microdomains, it is reasonable to propose that recruitment of phot1 to these regions facilitates receptor phosphorylation and coordinates signaling, at least for processes such as phototropism.

Taken together, our single-molecule analysis provided new insights into the regulation of the dynamics of phot1 at the PM with unprecedented spatial and temporal resolution. Our findings showed that under dark conditions, phot1 exhibited

heterogeneous dynamics and mainly existed as a monomer at the PM (Figure 7). When exposed to blue light, activated phot1 sequentially underwent dimerization and phosphorylation. More importantly, the phosphorylation of phot1 enhanced its interaction with AtRem1.3, and promoted faster movement of phot1. It will now be important to determine whether the microdomains identified here for phot1 relate to those reported for the phototropic signaling component NPH3 (Pedmale and Liscum, 2007) and whether phot1 recruitment to these membrane regions plays a role in initiating other phot1-mediated responses.

METHODS

Plant Materials and Transformation

Arabidopsis thaliana ecotype of Colombia-0 (Col-0) was used in all experiments. Seeds of *phot1-5* mutant and *PHOT1*$_{PRO}$*::PHOT1-GFP* (*phot1-5* background) transformed lines were obtained from Winslow Briggs (Carnegie Institution for Science, Stanford, CA). *GFP-LTi6a* transgenic lines were described elsewhere (Cutler et al., 2000). The *35S*$_{PRO}$*::PHOT1*^{D806N}*-GFP* transformation vectors were described previously (Kaiserli et al., 2009). The *PHOT1*^{D806N} coding sequence was obtained by digesting the vector with *Hind*III and *Bam*HI and then introducing the mutant coding sequence into the expression vector pEZR(K)-LC containing *PHOT1*$_{PRO}$*::PHOT1-GFP* to replace the wild-type *PHOT1* sequence. Thus, the *PHOT1*$_{PRO}$*::PHOT1*^{D806N}*-GFP* transformation vector was constructed and transformed into *phot1-5* mutants, and seedlings were selected with 50 μg/mL kanamycin. The genotype of the phot1^{D806N}-GFP line was determined by PCR, and the expression level was quantified by qPCR. Primers for mutant identification were 5’-ATGGAACCGATTGGTTTGAAGCATTTCA-3’ (forward) and 5’-AAAAACATTTGTTTGCAGATCTTCT-3’ (reverse). For qPCR, the primers were 5’-TCTTCTCACGATTGCTCCCAT-3’ (forward) and 5’-TGCTTGCTCACCTCCACTTGC-3’ (reverse) (Zhao et al., 2013). For dual-color

VA-TIRFM imaging, transgenic *PHOT1$_{PRO}$::PHOT1-GFP* lines were transformed with the vector containing *35S$_{PRO}$::AtRem1.3-mCherry*, and seedlings were selected with 50 μg/mL hygromycin.

Seeds were surface-sterilized with 70% EtOH (v/v) and 15% (v/v) H_2O_2 for 1 min; they were planted on plates containing half-strength Murashige and Skoog (MS) medium, 1% (w/v) sucrose and 1% (w/v) agar. Plates were vernalized at 4°C for 24 h and placed in a cultivation chamber at 22°C under a light regime of 16 h of white light/8 h of dark for light-grown seedlings. For DG seedlings, the plates were covered with aluminum foil following illumination with white light for 2 h at 22°C. For BL treatments in live-cell imaging, DG seedlings were first exposed to the indicated intensities of BL for indicated times and immediately observed by VA-TIRFM or confocal laser-scanning microscopy. For fixed cell imaging, seedlings were fixed in 4% (w/v) paraformaldehyde solution for 10 min.

Measurement of Phototropic Bending

For phototropism experiments without drug treatment, 3-d-old dark grown *phot1-GFP* seedlings grown on vertically oriented plates were irradiated with a unilateral blue LED (wavelength 470–490 nm) with an intensity of 0.5 μmol m^{-2} s^{-1} for 12 h. For measurements with MβCD treatment, 3-d-old DG seedlings grown on vertically oriented plates were pretreated with H_2O (control) or 10 mM MβCD for 30 min in the dark, and were transferred to a new plates containing 1/2× MS medium, 1% (w/v) sucrose, 1% (w/v) agar with or without (control) 10 mM MβCD under dim red light. Seedlings were then irradiated with unilateral blue LED (wavelength 470–490 nm) with an intensity of 1 μmol m^{-2} s^{-1} for 12 h. All operations were done under weak light provided by red LEDs in a dark room. A different and adjustable BL source for continuous BL illumination was provided by a LED with wavelength 470–490 nm. The intensity of BL was measured with a Sanwa power meter (model Sanwa LP1). Images were recorded with a digital camera at the indicated times. Angles between the

direction of the shoot tips and the vertical were measured manually with ImageJ software (National Institutes of Health, version 1.48).

MβCD Treatments

A solution of 10 mM MβCD (Sigma-Aldrich) was prepared in deionized water. 4-day-old DG seedlings were incubated in 1/2 × liquid MS medium containing MβCD for 30 min, then transferred onto a slide with MβCD solution and covered with a coverslip for VA-TIRFM imaging. For sterol complementation, campesterol and β-sitosterol were dissolved in chloroform to yield 50 mg/mL stock solutions. Vertically grown 4-d-old seedlings were incubated in 1/2× MS medium containing 100 μg/mL campesterol or β-sitosterol for 60 min following MβCD treatment.

FRAP Analysis

An FV1000MPE multiphoton laser-scanning microscope (Olympus) was applied to perform the FRAP experiments. The circular region of interest (ROI) was drawn and bleached with a 488-nm laser at 100% laser power. The time interval for monitoring fluorescence recovery was 3 s. The fluorescence recovery was quantified using ImageJ software (National Institutes of Health). The data obtained were corrected for bleaching during imaging as described (Luu et al., 2012). Origin 8.6 software (OriginLab Corporation) was used for curve fitting.

BiFC Analysis

The coding region of *Arabidopsis PHOT1* was cloned by PCR via *Kpn*I and *Bam*HI restriction sites into modified *pCAMBIA 2300* vectors containing *35S::nYFP* or *35S::cYFP* to create fusion proteins with the N- and C-terminal halves of YFP at the C-terminus of phot1 or phot1^{D806N}, respectively. *Agrobacterium tumefaciens* GV3101 carrying both constructs were infiltrated into the abaxial side of *Nicotiana tabacum L.* leaves (OD_{600} = 0.5:0.5). Plants were incubated under white light for 24 h and then kept in the dark for 24 h prior to imaging. The leaves were observed using a Leica TCS SP5 laser scanning microscope with a 514-nm laser. The fluorescence intensity

was quantified with ImageJ software (National Institutes of Health, version 1.48).

FRET-FLIM Analysis

For FRET-FLIM analysis, seedlings were immediately fixed in 4% (w/v) paraformaldehyde after the indicated treatments. FLIM was performed on an inverted OLYMPUS FV1200 microscope equipped with a Picoquant picoHarp300 (Germany) controller. The excitation at 488 nm was carried out by a picosecond pulsed diode laser at a repetition rate of 40 MHz, through a water immersion objective (60×, N.A. 1.2). The emitted light was filtered with a 520/35 nm bandpass filter and detected by a MPD SPAD detector. Images with the selected ROI were acquired with acquisition photons of up to 20000. From the fluorescence intensity images, the decay curves were calculated per pixel and fitted with either a mono- or double-exponential decay model using the SymphoTime 64 software (PicoQuant, Germany). The mono-exponential model function was applied for donor samples with only GFP present. The double-exponential model function was used for sample containing GFP and mCherry.

Single-Particle Imaging, Tracking, and Analysis

DG seedlings were mounted between a glass slide and a cover slip with 1/2 liquid MS medium and then observed with a home-built objective-type VA-TIRFM, which was based on an inverted microscope (Olympus IX-71) equipped with a TIRF illumination module (Olympus IX2-RFAEVA-2) and a 100× oil-immersion objective (Olympus PlanApo, NA 1.45). Proteins labeled with GFP or mCherry were excited with 473-nm or 561-nm laser lines, and two band-pass filters (525/34 and 609/54) were applied to pass through the emission fluorescence signals. A back-illuminated EM-CCD camera (ANDOR iXon DV8897D-CS0-VP) was used for recording. Image acquisition was controlled by Micro-Manager together with ImageJ software (National Institutes of Health, version 1.48), with an exposure time of 200 ms. For treatment with BL, the blue LED was placed and fixed on the object stage. During the experiment, the

seedlings were first mounted on the microscope and then exposed to the light. The time-lapse images were recorded right after the light treatments.

Images were processed by a wavelet transform algorithm with an appropriate threshold (Olivo-Marin, 2002). The position of particles was determined by calculating the weighted-centroid with sub-pixel accuracy following determination of the local maxima with a mask of 5 × 5 pixels. Single particle tracking was performed according to spatial and temporal global particle assignment as described previously (Jaqaman et al., 2008). Trajectories with length > 2 frames were kept for surface dwell time analysis, and those with length > 14 frames were kept for MSD, diffusion coefficient, and motion range analysis. For each track, the MSD was calculated using the following formula:

$$\mathrm{MSD(t)} = \frac{1}{\mathrm{L-n}}\sum_{\mathrm{s=0}}^{\mathrm{L-n-1}}(\mathrm{r(s+n)} - \mathrm{r(s)})^2 \qquad \text{[S1]}$$

where $n = t/\Delta t$, L is the length of the trajectory and $r(s)$ is the two-dimensional position of the particle in frames (Goulian and Simon, 2000). The diffusion coefficient for a spot was determined by fitting a line to MSD with n running from 1 to the largest integer $\leq L/4$ (Goulian and Simon, 2000). The motion range was computed as the largest displacement during the particle's lifetime. The confinement area was calculated by fitting the data of plotting MSD against time (t) with the formula below:

$$\mathrm{MSD} = \frac{A^2}{3}\left[1 - exp\left(\frac{-12Dt}{A^2}\right)\right] \qquad \text{[S2]}$$

Where A^2 is the confinement area (in μm^2) as described (Mercer et al., 2012).

The Progressive Idealization and Filtering (PIF) program was used for step-wise photobleaching analysis. After background subtraction by the rolling ball method in ImageJ software, images were input into the PIF program and subjected to the steps described previously (McGuire et al., 2012).

In the process of spatial intensity distribution analysis (SpIDA), white noise was measured with ImageJ software. The standalone MATLAB Graphical User Interface

program was then used for SpIDA analysis in accordance with the user guide (program is available at the Neurophotonics web site: www.neurophotonics.ca/tools/software.html) (Godin et al., 2011).

Protein Extraction and Immunoblotting Analysis

4-day-old DG *Arabidopsis* seedlings were grown and treated under different conditions as described above. Samples were ground to a fine powder in liquid nitrogen, mixed with buffer E (125 mM Tris-HCl pH 8.8, 1% (w/v) SDS, 10% (v/v) glycerol, 50 mM $Na_2S_2O_5$), and centrifuged at 13000 × g for 10 min; the supernatant was saved. Aliquots of 20 μL of the supernatant from each sample were used to determine protein concentration, and the remainder was diluted with 1/10 volume of buffer Z (125 mM Tris-HCl pH 6.8, 12% (w/v) SDS, 10% (v/v) glycerol, 22% (v/v) β-mercaptoethanol, 0.0001% (w/v) bromophenol blue). The samples were then separated on 6% SDS/polyacrylamide gels containing 20 μM Phos-tag Acrylamide (Boppard) and 10 μM $MnCl_2$ and transferred onto polyvinylidene fluoride membranes (Pall) by electroblotting. Immunoblotting analysis was performed with anti-phot1 antibody.

Accession Numbers

Sequence data from this article can be found in the *Arabidopsis* Information Resource (TAIR) database under the following accession numbers: *PHOT1* (AT3G45780), *AtRem1.3* (At2g45820).

FUNDING

This work is supported by the National Natural Science Foundation of China (31530084, 31270224) and the Program of Introducing Talents of Discipline to Universities (111 project, B13007).

AUTHOR CONTRIBUTIONS

Y.X., J.X., Y.W., J.M.C., and J.L. designed research; Y.X., J.X., X.L., L.F., and K.S.

performed research; L.F., Y.Z. and X.W. contributed new reagents/analytic tools; Y.X., Y.W., J.X., X.L., L.F., K.S., Y.Z., L.W. and J.M.C. analyzed the data, Y.X., J.X., Y.W., K.S., X.W., X.D., F.B., J.M.C. and J.L. wrote the paper.

The authors declare no conflict of interest.

ACKNOWLEDGMENTS

We thank Prof. Winslow Briggs (Carnegie Institution for Science) for kindly providing some transgenic materials and mutants, and Dr. Yong Wu (University of California) for guiding the PPI analysis. We thank the Imaging Core Facility, Technology Center for Protein Sciences, Tsinghua University for assistance with using FV1200 LSCM with Picoquant FLIM/FCS system.

REFERENCES

Bucherl, C.A., Bader, A., Westphal, A.H., Laptenok, S.P., and Borst, J.W. (2014). FRET-FLIM applications in plant systems. Protoplasma **251**:383-394.

Christie, J.M. (2007). Phototropin blue-light receptors. Annu. Rev. Plant Biol. **58**:21-45.

Ciesla, J., Fraczyk, T., and Rode, W. (2011). Phosphorylation of basic amino acid residues in proteins: important but easily missed. Acta Biochim. Pol. **58**:137-148.

Corriden, R., Kilpatrick, L.E., Kellam, B., Briddon, S.J., and Hill, S.J. (2014). Kinetic analysis of antagonist-occupied adenosine-A3 receptors within membrane microdomains of individual cells provides evidence of receptor dimerization and allosterism. FASEB J. **28**:4211-4222.

Cutler, S.R., Ehrhardt, D.W., Griffitts, J.S., and Somerville, C.R. (2000). Random GFP::cDNA fusions enable visualization of subcellular structures in cells of *Arabidopsis* at a high frequency. Proc. Natl. Acad. Sci. USA **97**:3718-3723.

Das, S.K., Darshi, M., Cheley, S., Wallace, M.I., and Bayley, H. (2007). Membrane protein stoichiometry determined from the step-wise photobleaching of dye-labelled subunits. Chembiochem **8**:994-999.

Demir, F., Horntrich, C., Blachutzik, J.O., Scherzer, S., Reinders, Y., Kierszniowska, S., Schulze,

W.X., Harms, G.S., Hedrich, R., Geiger, D., et al. (2013). *Arabidopsis* nanodomain-delimited ABA signaling pathway regulates the anion channel SLAH3. Proc. Natl. Acad. Sci. USA **110**:8296-8301.

George, S.R., Fan, T., Xie, Z., Tse, R., Tam, V., Varghese, G., and O'Dowd, B.F. (2000). Oligomerization of mu- and delta-opioid receptors. Generation of novel functional properties. J. Biol. Chem. **275**:26128-26135.

Godin, A.G., Costantino, S., Lorenzo, L.E., Swift, J.L., Sergeev, M., Ribeiro-da-Silva, A., De Koninck, Y., and Wiseman, P.W. (2011). Revealing protein oligomerization and densities in situ using spatial intensity distribution analysis. Proc. Natl. Acad. Sci. USA **108**:7010-7015.

Goulian, M., and Simon, S.M. (2000). Tracking single proteins within cells. Biophys. J. **79**:2188-2198.

Hartmann, M.A. (1998). Plant sterols and the membrane environment. Trends Plant Sci. **3:** 170-175.

Hohm, T., Preuten, T., and Fankhauser, C. (2013). Phototropism: translating light into directional growth. Am. J. Bot. **100**:47-59.

Inoue, S., Kinoshita, T., Matsumoto, M., Nakayama, K.I., Doi, M., and Shimazaki, K. (2008). Blue light-induced autophosphorylation of phototropin is a primary step for signaling. Proc. Natl. Acad. Sci. USA **105**:5626-5631.

Jaqaman, K., Loerke, D., Mettlen, M., Kuwata, H., Grinstein, S., Schmid, S.L., and Danuser, G. (2008). Robust single-particle tracking in live-cell time-lapse sequences. Nat. Methods **5**:695-702.

Jarsch, I.K., Konrad, S.S., Stratil, T.F., Urbanus, S.L., Szymanski, W., Braun, P., Braun, K.H., and Ott, T. (2014). Plasma membranes are subcompartmentalized into a plethora of coexisting and diverse microdomains in *Arabidopsis* and *Nicotiana benthamiana*. Plant Cell **26**:1698-1711.

Kaiserli, E., Sullivan, S., Jones, M.A., Feeney, K.A., and Christie, J.M. (2009). Domain swapping to assess the mechanistic basis of *Arabidopsis* phototropin 1 receptor kinase activation and endocytosis by blue light. Plant Cell **21**:3226-3244.

Katsura, H., Zikihara, K., Okajima, K., Yoshihara, S., and Tokutomi, S. (2009). Oligomeric structure of LOV domains in *Arabidopsis* phototropin. FEBS Lett. **583**:526-530.

Knieb, E., Salomon, M., and Rudiger, W. (2005). Autophosphorylation, electrophoretic mobility and immunoreaction of oat phototropin 1 under UV and blue Light. Photochem. Photobiol.

81:177-182.

Li, X., Luu, D.T., Maurel, C., and Lin, J. (2013). Probing plasma membrane dynamics at the single-molecule level. Trends Plant Sci. **18**:617-624.

Liscum, E., and Briggs, W.R. (1995). Mutations in the NPH1 locus of *Arabidopsis* disrupt the perception of phototropic stimuli. Plant Cell **7**:473-485.

Long, Y., Stahl, Y., Weidtkamp-Peters, S., Postma, M., Zhou, W., Goedhart, J., Sanchez-Perez, M.I., Gadella, T.W.J., Simon, R., Scheres, B., et al. (2017). In vivo FRET-FLIM reveals cell-type-specific protein interactions in Arabidopsis roots. Nature **548**:97-102.

Luu, D.T., Martiniere, A., Sorieul, M., Runions, J., and Maurel, C. (2012). Fluorescence recovery after photobleaching reveals high cycling dynamics of plasma membrane aquaporins in *Arabidopsis* roots under salt stress. Plant J. **69**:894-905.

Malinsky, J., Opekarova, M., Grossmann, G., and Tanner, W. (2013). Membrane microdomains, rafts, and detergent-resistant membranes in plants and fungi. Annu. Rev. Plant Biol.**64**:501-529.

Marianayagam, N.J., Sunde, M., and Matthews, J.M. (2004). The power of two: protein dimerization in biology. Trends Biochem. Sci. **29**:618-625.

Matsuoka, D., Iwata, T., Zikihara, K., Kandori, H., and Tokutomi, S. (2007). Primary processes during the light-signal transduction of phototropin. Photochem. Photobiol. **83**:122-130.

McGuire, H., Aurousseau, M.R., Bowie, D., and Blunck, R. (2012). Automating single subunit counting of membrane proteins in mammalian cells. J. Biol. Chem. **287**:35912-35921.

Mercer, A.J., Szalewski, R.J., Jackman, S.L., Van Hook, M.J., and Thoreson, W.B. (2012). Regulation of presynaptic strength by controlling Ca^{2+} channel mobility: effects of cholesterol depletion on release at the cone ribbon synapse. J. Neurophysiol. **107**:3468-3478.

Mo, M., Yokawa, K., Wan, Y., and Baluska, F. (2015). How and why do root apices sense light under the soil surface? Front. Plant Sci. **6**:775.

Nakasako, M., Iwata, T., Matsuoka, D., and Tokutomi, S. (2004). Light-induced structural changes of LOV domain-containing polypeptides from *Arabidopsis* phototropin 1 and 2 studied by small-angle X-ray scattering. Biochemistry **43**:14881-14890.

Olivo-Marin, J.C. (2002). Extraction of spots in biological images using multiscale products. Pattern Recogn. **35**:1989-1996.

Pedmale, U.V., and Liscum, E. (2007). Regulation of phototropic signaling in Arabidopsis via

phosphorylation state changes in the phototropin 1-interacting protein NPH3. J. Biol. Chem. **282**:19992-20001.

Preuten, T., Blackwood, L., Christie, J.M., and Fankhauser, C. (2015). Lipid anchoring of *Arabidopsis* phototropin 1 to assess the functional significance of receptor internalization: should I stay or should I go? New Phytol. **206**:1038-1050.

Roche, Y., Gerbeau-Pissot, P., Buhot, B., Thomas, D., Bonneau, L., Gresti, J., Mongrand, S., Perrier-Cornet, J.M., and Simon-Plas, F. (2008). Depletion of phytosterols from the plant plasma membrane provides evidence for disruption of lipid rafts. FASEB J. **22:** 3980-3991.

Sakai, T., Kagawa, T., Kasahara, M., Swartz, T.E., Christie, J.M., Briggs, W.R., Wada, M., and Okada, K. (2001). *Arabidopsis* nph1 and npl1: blue light receptors that mediate both phototropism and chloroplast relocation. Proc. Natl. Acad. Sci. USA **98**:6969-6974.

Sakamoto, K., and Briggs, W.R. (2002). Cellular and subcellular localization of phototropin 1. Plant Cell **14**:1723-1735.

Schlessinger, J. (2002). Ligand-induced, receptor-mediated dimerization and activation of EGF receptor. Cell **110**:669-672.

Song, K., Xue, Y., Wang, X., Wan, Y., Deng, X., and Lin, J. (2017). A modified GFP facilitates counting membrane protein subunits by step-wise photobleaching in *Arabidopsis*. J. Plant Physiol. **213**:129-133.

Sun, Y., Li, N., and Fang, X. (2015). Probing the dynamics of growth factor receptor by single-molecule fluorescence imaging. Prog. Biophys. Mol. Biol. **118**:95-102.

Tinoco, I. Jr., and Gonzalez, R.L., Jr. (2011). Biological mechanisms, one molecule at a time. Genes Dev. **25**:1205-1231.

Titapiwatanakun, B., Blakeslee, J.J., Bandyopadhyay, A., Yang, H., Mravec, J., Sauer, M., Cheng, Y., Adamec, J., Nagashima, A., Geisler, M., et al. (2009). ABCB19/PGP19 stabilises PIN1 in membrane microdomains in Arabidopsis.Plant J. **1**:27-44.

Ueda, M., Sako, Y., Tanaka, T., Devreotes, P., and Yanagida, T. (2001). Single-molecule analysis of chemotactic signaling in *Dictyostelium* cells. Science **5543**:864-867.

Ulbrich, M.H., and Isacoff, E.Y. (2007). Subunit counting in membrane-bound proteins. Nat. Methods **4**:319-321.

Wan, Y., Ash, W.M., 3rd, Fan, L., Hao, H., Kim, M.K., and Lin, J. (2011). Variable-angle total

internal reflection fluorescence microscopy of intact cells of *Arabidopsis thaliana*. Plant Methods **7**:27.

Wan, Y. Jasik J., Wang L, Hao H, Volkmann D, Menzel D, Mancuso S, Baluška F, Lin J. (2012). The signal transducer NPH3 integrates the phototropin1 photosensor with PIN2-based polar auxin transport in *Arabidopsis* root phototropism. Plant Cell 24: 551-565.

Wan, Y.L., Eisinger, W., Ehrhardt, D., Kubitscheck, U., Baluska, F., and Briggs, W. (2008). The subcellular localization and blue-light-induced movement of phototropin 1-GFP in etiolated seedlings of *Arabidopsis thaliana*. Mol. Plant **1**:103-117.

Wang, X., Li, X., Deng, X., Luu, D.T., Maurel, C., and Lin, J. (2015). Single-molecule fluorescence imaging to quantify membrane protein dynamics and oligomerization in living plant cells. Nat. Protoc. **10**:2054-2063.

Wu, Y., Eghbali, M., Ou, J., Lu, R., Toro, L., and Stefani, E. (2010). Quantitative determination of spatial protein-protein correlations in fluorescence confocal microscopy. Biophys. J. **98**:493-504.

Yadeta, K.A., Elmore, J.M., and Coaker, G. (2013). Advancements in the analysis of the *Arabidopsis* plasma membrane proteome. Front. Plant Sci. **4**:86.

Zhao, X., Wang, Y.L., Qiao, X.R., Wang, J., Wang, L.D., Xu, C.S., and Zhang, X. (2013). Phototropins function in high-intensity blue light-induced hypocotyl phototropism in *Arabidopsis* by altering cytosolic calcium. Plant Physiol. **162**:1539-1551.

Zidovetzki, R., and Levitan, I. (2007). Use of cyclodextrins to manipulate plasma membrane cholesterol content: Evidence, misconceptions and control strategies. BBA-Biomembranes **1768**:1311-1324.

Zinchuk, V., Wu, Y., Grossenbacher-Zinchuk, O., and Stefani, E. (2011). Quantifying spatial correlations of fluorescent markers using enhanced background reduction with protein proximity index and correlation coefficient estimations. Nat. Protoc. **6**:1554-1567.

FIGURE LEGENDS

Figure 1. Dynamics of phot1-GFP at the PM under DG Conditions.

(A) VA-TIRFM image of a DG hypocotyl cell expressing phot1-GFP. Circles indicate the positions of spots apeared or will appear.

(B) Montage of circles depicted in **(A)**.

(C) Fluorescence intensity profiles of the four spots depicted in **(A)** and **(B)**.

(D) Surface dwell time (lifetime) distribution of phot1-GFP spots (n = 529 spots).

(E) Distribution of diffusion coefficients of phot1-GFP spots (n = 550 spots).

(F) Distribution of motion ranges of phot1-GFP spots (n = 526 spots).

(G) Ratio (blue circle, n = 498 spots) and density (red square, n = 7 hypocotyls) distribution of phot1 monomer and dimer. Error bars represent the SD.

Scale bars: **A** and **B**, 5 μm.

Figure 2. Dynamics of phot1-GFP at the PM under Different BL Conditions.

(A) Surface dwell time distribution of phot1-GFP spots under BL-60 (n = 611 spots), BL-600 (n = 608 spots), and BL-6000 conditions (n = 586 spots).

(B) Distribution of diffusion coefficients of phot1-GFP spots under BL-60 (n = 531 spots), BL-600 (n = 529 spots), and BL-6000 conditions (n = 537 spots).

(C) Distribution of motion ranges of phot1-GFP spots under BL-60 (n = 559 spots), BL-600 (n = 529 spots), and BL-6000 conditions (n = 546 spots).

(D) Step distribution of phot1-GFP spots BL-60 (n = 633 spots), BL-600 (n = 476 spots), and BL-6000 (n = 540 spots) conditions.

(E) Density distribution of phot1-GFP spots under BL-60 (n = 7 hypocotyls), BL-600 (n = 8 hypocotyls) and BL-6000 conditions (n = 8 hypocotyls). $^{*}P < 0.05$, $^{**}P < 0.01$, $^{***}P < 0.001$. Student's t test. Error bars represent the SD.

Figure 3. Partitioning of phot1-GFP is Associated with Membrane Microdomains.

(A–C) VA-TIRFM images of hypocotyl epidermal cells of DG seedling expressing phot1-GFP **(A)** and AtRem1.3-mCherry **(B)** and merge **(C)**. Foci with only GFP or mCherry fluorescence are indicated by green or red circles, respectively. Foci with both GFP and mCherry fluorescence are indicated by yellow circles.

(D–E) Kymograph representation of the time course of colocalized foci (yellow arrowhead) and non-colocalized foci (green and red arrowheads indicate the foci containing only GFP or mCherry fluorescence, respectively).

Horizontal scale bars: **A**, 5 μm; **D** and **E**, 3 μm; vertical scale bars: 10 s.

Figure 4. Analysis of phot1-GFP and AtRem1.3-mCherry Colocalization and Interaction at the PM.

(A–B) Time lapse **(A)** and kymograph **(B)** showing the dimerization of two phot1-GFP spots, one of which colocalized with AtRem1.3-mCherry (white circles).

(C) Effects of MβCD on the photobleaching step distribution of phot1-GFP on the PM of DG hypocotyl cells under DG (*n* = 685 spots) and BL-6000 (*n* = 683 spots) conditions.

(D) Fluorescence lifetime image of phot1-GFP under DG conditions.

(E–G) Fluorescence lifetime image of phot1-GFP in the presence of AtRem1.3-mCherry under DG conditions **(E)** and BL (10 μmol m^{-2} s^{-1}) for 10 min **(F)** and 30 min **(G)**. The color bar represents the false color code for phot1-GFP fluorescence lifetimes.

(H) Time course of phot1-GFP and AtRem1.3-mCherry association in seedlings treated with BL (10 μmol m^{-2} s^{-1}). Error bars represent the SD.

Horizontal scale bars: **A** and **B**, 2 μm; **D–G**, 5 μm; vertical bars: **B**, 10 s.

Figure 5. BL-induced Dynamics of Kinase-inactive phot1.

(A) Distribution of diffusion coefficients of $phot1^{D806N}$-GFP under DG (n = 568 spots) and BL-6000 (*n* = 549 spots) conditions.

(B) Distribution of motion ranges of phot1^{D806N}-GFP under DG (n = 567 spots) and BL-6000 conditions (n = 576 spots).

(C) Time course of FRAP of phot1-GFP and phot1^{D806N}-GFP. Circles indicate the region that was photobleached.

(D–E) FRAP analysis of phot1-GFP **(D)** and phot1^{D806N}-GFP **(E)**. Curves represent the mean values of 6 hypocotyls for phot1-GFP or phot1^{D806N}-GFP. $^{***}P < 0.001$, Student's t test. Error bars represent the SD.

Scale bars: **C**, 10 μm.

Figure 6. Molecular Interactions of phot1^{D806N} and Effect of MβCD on phot1 Autophosphorylation.

(A) BiFC analysis of phot1 and phot1^{D806N} interaction.

(B) Quantification of relative YFP fluorescence intensity in tobacco epidermal cells. Error bars represent the SD from at least three independent experiments for each group.

(C) Photobleaching steps of phot1^{D806N}-GFP under DG (n = 592 spots) and BL-6000 (n = 633 spots) conditions. $^{**}P < 0.01$. Student's t test.

(D) Effects of MβCD on phot1 kinase activity in protein extracts from *Arabidopsis* seedlings.

Scale bars: **A**, 20 μm.

Figure 7. Hypothetical Model of Phot1 Activation in Membrane Microdomains in Response to BL in *Arabidopsis*.

Under dark conditions, phot1 is inactive state that mainly exists as a monomer at the PM, partly associated with AtRem1.3-labeled microdomains. After blue light exposure, activated phot1 sequentially undergoes dimerization and phosphorylation. The latter enhances phot1 assembly in membrane microdomains, interaction with AtRem1.3, and also promotes faster movement of phot1.

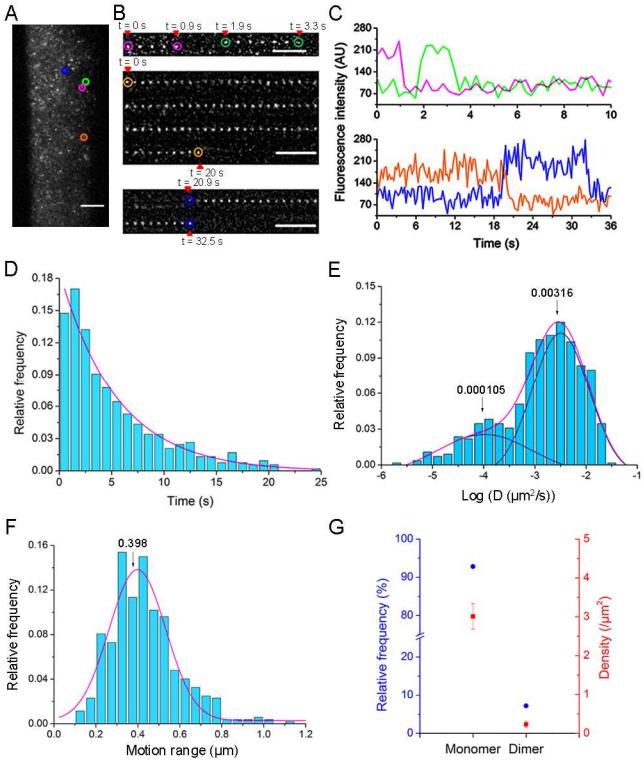
A
B
t = 0 s
t = 0.9 s
t = 1.9 s
t = 3.3 s
t = 0 s
t = 20 s
t = 20.9 s
t = 32.5 s
C
Fluorescence intensity (AU)
Time (s)
D
Relative frequency
Time (s)
E
0.00316
0.000105
Relative frequency
Log (D (μm²/s))
F
0.398
Relative frequency
Motion range (μm)
G
Relative frequency (%)
Density (/μm²)
Monomer
Dimer

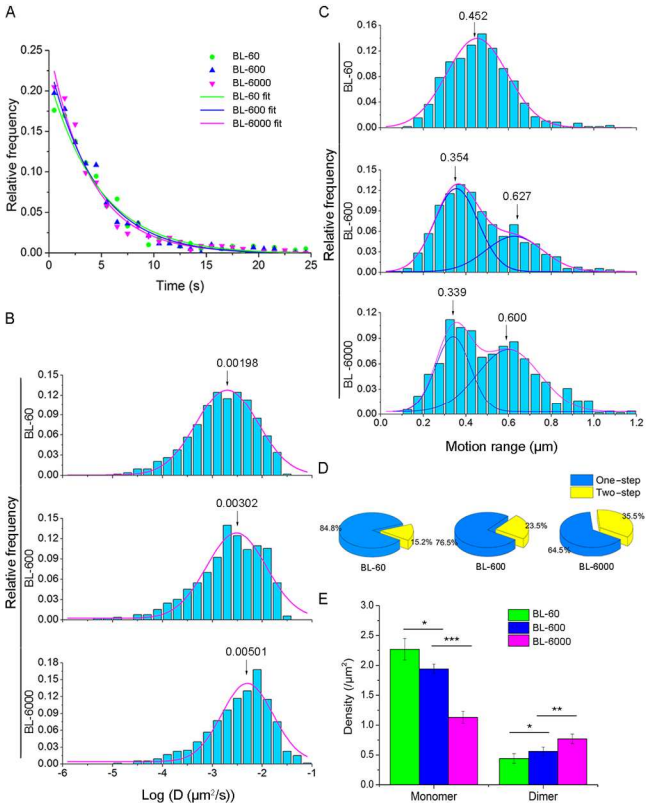
A
Relative frequency
Time (s)
BL-60
BL-600
BL-6000
BL-60 fit
BL-600 fit
BL-6000 fit
B
Relative frequency
Log (D (μm²/s))
0.00198
0.00302
0.00501
BL-60
BL-600
BL-6000
C
Relative frequency
Motion range (μm)
0.452
0.354
0.627
0.339
0.600
D
One-step
Two-step
84.8%
15.2%
76.5%
23.5%
64.5%
35.5%
E
Density (/μm²)
Monomer
Dimer
*
***
**

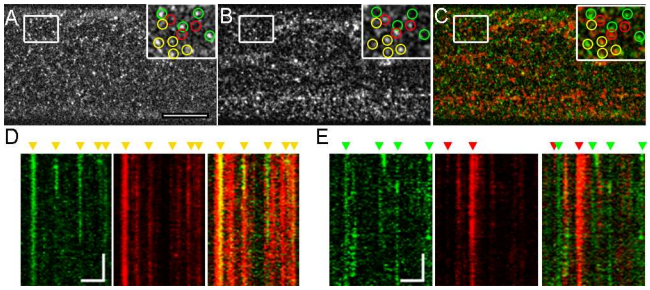
A
B
C

D
E

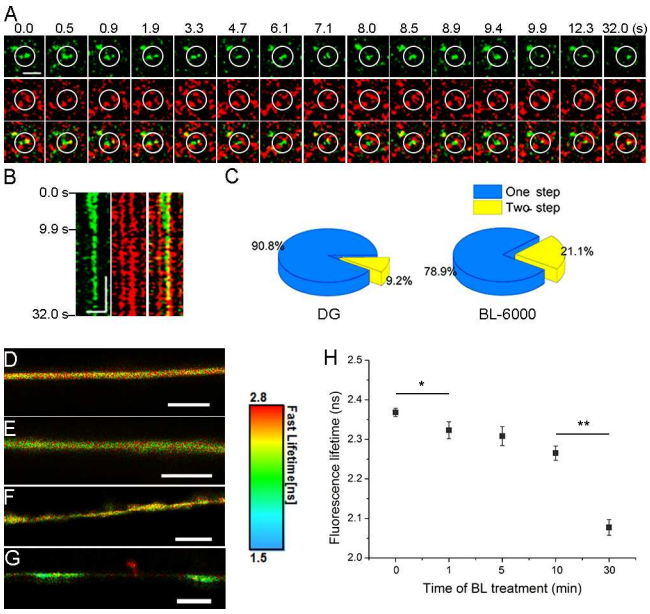
A
0.0
0.5
0.9
1.9
3.3
4.7
6.1
7.1
8.0
8.5
8.9
9.4
9.9
12.3
32.0 (s)
B
0.0 s
9.9 s
32.0 s
C
One step
Two step
90.8%
9.2%
78.9%
21.1%
DG
BL-6000
D
E
F
G
2.8
Fast Lifetime[ns]
1.5
H
Fluorescence lifetime (ns)
2.5
2.4
2.3
2.2
2.1
2.0
*
**
0
1
5
10
30
Time of BL treatment (min)

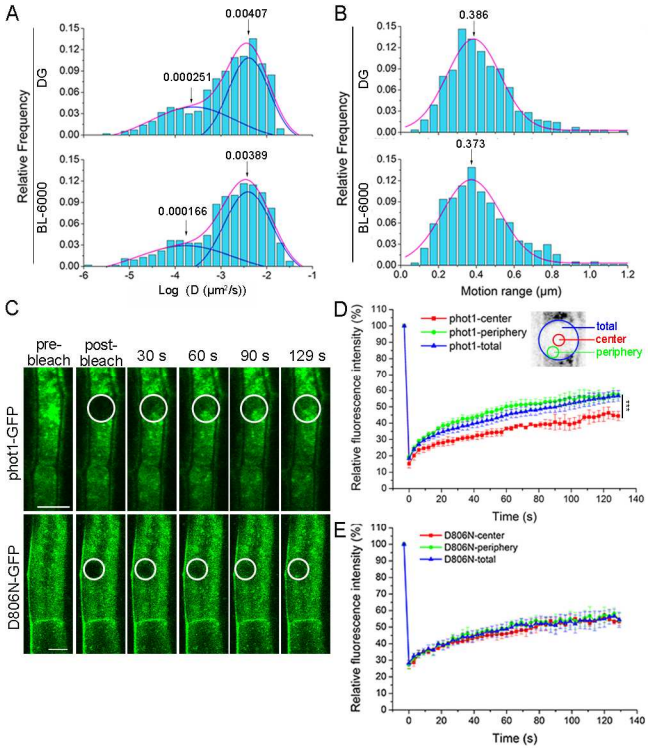
A
B
C
D
E
Relative Frequency
DG
BL-6000
0.00407
0.000251
0.00389
0.000166
Log (D (μm²/s))
0.386
0.373
Motion range (μm)
pre-bleach
post-bleach
30 s
60 s
90 s
129 s
phot1-GFP
D806N-GFP
phot1-center
phot1-periphery
phot1-total
total
center
periphery
Relative fluorescence intensity (%)
Time (s)
D806N-center
D806N-periphery
D806N-total

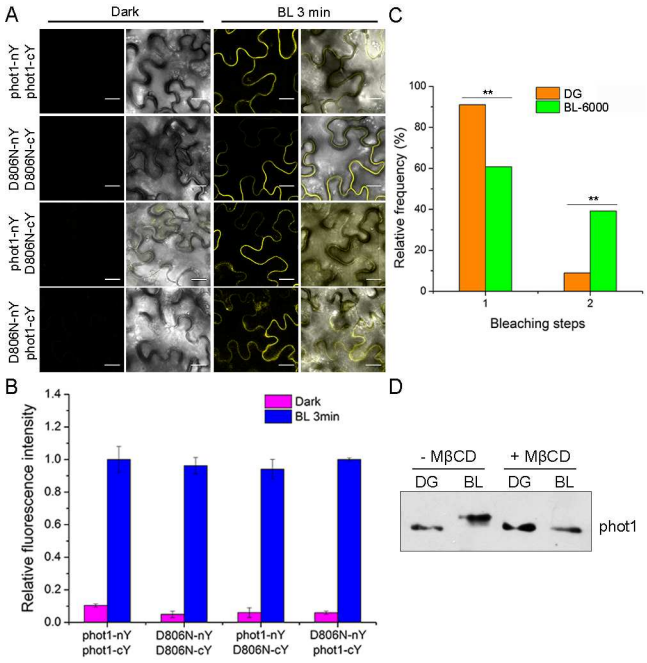
A
Dark
BL 3 min
phot1-nY
phot1-cY
D806N-nY
D806N-cY
phot1-nY
D806N-cY
D806N-nY
phot1-cY
C
DG
BL-6000
Relative frequency (%)
Bleaching steps
**
**
B
Dark
BL 3min
Relative fluorescence intensity
phot1-nY
phot1-cY
D806N-nY
D806N-cY
phot1-nY
D806N-cY
D806N-nY
phot1-cY
D
- MβCD
+ MβCD
DG
BL
DG
BL
phot1

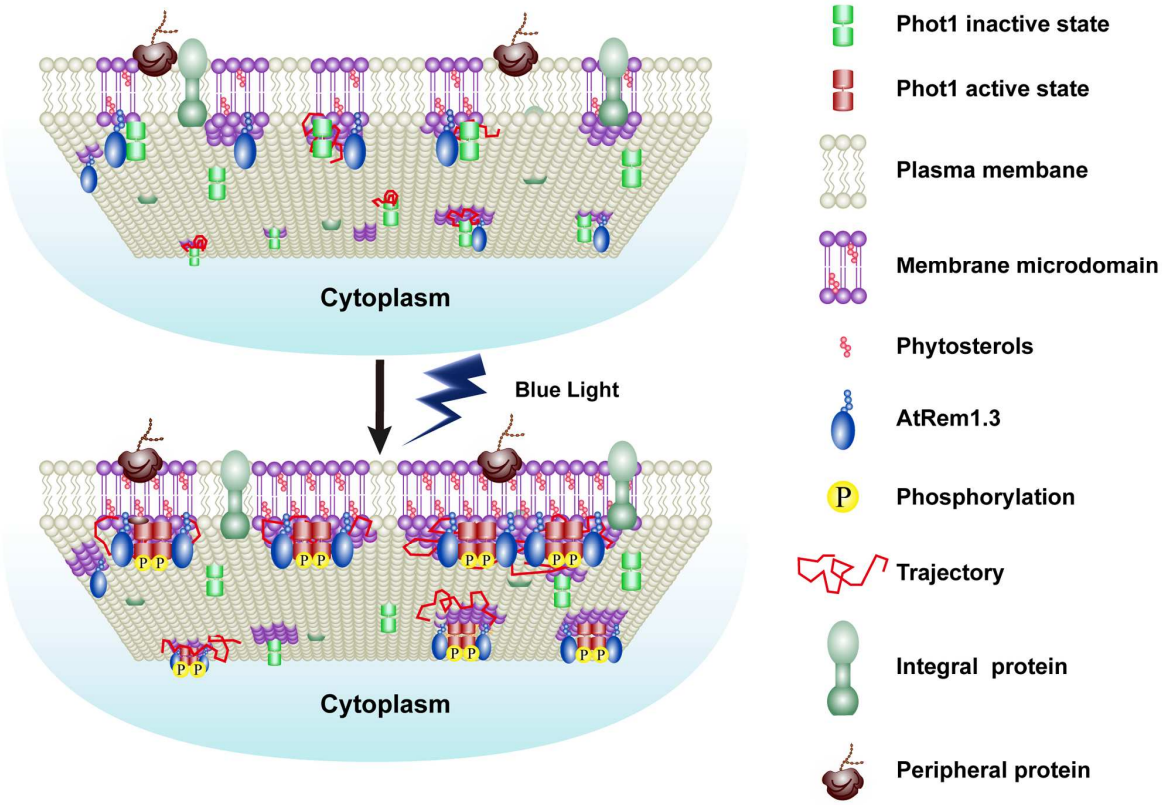
Cytoplasm
Blue Light
Cytoplasm
Phot1 inactive state
Phot1 active state
Plasma membane
Membrane microdomain
Phytosterols
AtRem1.3
Phosphorylation
Trajectory
Integral protein
Peripheral protein